THE PUBLISHING HOUSE
OF THE ROMANIAN ACADEMY

PROCEEDINGS OF THE ROMANIAN ACADEMY, Series A,
Volume 17, Number 1/2016, pp. 67–75

INVERSE DYNAMICS AND SIMULATION OF A 5-DOF MODULAR PARALLEL ROBOT USED IN BRACHYTHERAPY

Nicolae PLITEA, Andras SZILAGHYI, Dragos COCOREAN, Calin VAIDA, Doina PISLA

CESTER – Research Centre for Industrial Robots Simulation and Testing, Technical University of Cluj-Napoca, Romania
Corresponding author: Calin VAIDA, E-mail: calin.vaida@mep.utcluj.ro

Abstract. The paper presents the dynamic behavior of a 5-DOF parallel robot. The innovative modular structure was developed for medical use, especially in brachytherapy for the precise positioning of the BT needles in any part of the patient body. The dynamic model presented in this paper will enable the development of adequate control algorithms to fulfill the accuracy requirements for the task in hand. Knowing the general motion of the end-effector, the inverse dynamics problem is solved using an approach based on the general principle of virtual work. Finally the achieved results are compared with the Siemens NX dynamic simulations.

Key words: parallel robot, dynamics, principle of virtual work, modular structure, brachytherapy.

LIST OF SYMBOLS

$q=[q_1,q_2,q_3,q_4,q_5]^T$ – vector of the active joint coordinates;
$K(X_K,Y_K,Z_K,\psi_K,\theta_K)$ – Point vector defined by spatial parameters;
$l_k,d_k,e_k,h_k,\alpha_k,\varphi_k,\gamma_k$ – length and angular parameters;
$\delta q=[\delta q_1,\delta q_2,\delta q_3,\delta q_4,\delta q_5]^T$ – vector of virtual displacements of the active joint positions;
$X_E=[X_E,Y_E,Z_E]^T$ – position vector of a characteristic point of the end-effector;
$\delta X_E=[\delta X_E,\delta Y_E,\delta Z_E]^T$ – vector of the virtual displacements of the *E* point;
$X_{m_i}=[X_i,Y_i,Z_i]^T$, $i=1...28$ – vector of coordinates of the lumped masses m_i;
$\delta X_{m_i}=[\delta X_i,\delta Y_i,\delta Z_i]^T$ – vector of the virtual displacements of the m_i points;
$\tau=[\tau_1,\tau_2,\tau_3,\tau_4,\tau_5]^T=[F_1,Mo_2,F_3,Mo_4,F_5]^T$ – vector of active forces/moments;

$$J_i=\begin{bmatrix}\frac{\partial X_i}{\partial q_1} & \frac{\partial X_i}{\partial q_2} & \frac{\partial X_i}{\partial q_3} & \frac{\partial X_i}{\partial q_4} & \frac{\partial X_i}{\partial q_5}\\ \frac{\partial Y_i}{\partial q_1} & \frac{\partial Y_i}{\partial q_2} & \frac{\partial Y_i}{\partial q_3} & \frac{\partial Y_i}{\partial q_4} & \frac{\partial Y_i}{\partial q_5}\\ \frac{\partial Z_i}{\partial q_1} & \frac{\partial Z_i}{\partial q_2} & \frac{\partial Z_i}{\partial q_3} & \frac{\partial Z_i}{\partial q_4} & \frac{\partial Z_i}{\partial q_5}\end{bmatrix},\ i=1...28,$$

– the generalised Jacobi matrix defining the transformation between velocity vector of *E* point and the velocity vector of the active joints.

1. INTRODUCTION

Brachytherapy (BT) is a form of radiotherapy where radiation sources (in form of small sized seeds) are placed inside or next to the area requiring treatment, using rigid needles with diameters of 1.6 mm up to 2 mm and a length up to 250 mm. BT represents the therapeutic index in prostate cancer [1] but even though it proved its efficiency in the treatment of cervical, prostate, breast and skin cancer its spread is limited due

to its high accuracy positioning requirements. Reference is made to the overview study [2] published in 2010 during the annual meeting of the AAPM (American Association of Physicists in Medicine), where the 13 robotic systems developed for prostate brachytherapy were presented, stating the potential of robotic systems in BT and the need for the development of a robotic system with a high degree of universality, capable of working in different cancer scenarios. This research opportunity was addressed by the authors who propose an innovative 5-DOF parallel robotic structure capable to target any tumor located in the thoracic-abdominal area of the body. The required accuracy for the procedure accepts a maximum error of 1 mm with regard to the targeted point, which is very challenging due to several aspects: tissue elasticity; needle deformability; the variable density and specific penetration resistance of the different tissues that have to be pierced; the correlation between the robot workspace and the application task [3].

H. Bassan built a 5-DOF hybrid robotic system to perform 3D ultrasound guided percutaneous needle insertion surgery [4]. The macro stage is responsible for the orientation of the needle with parallel mechanism and the micro stage for needle insertion and rotation. Yu *et al.* presents a 16 degrees-of-freedom robotic system, 9 DOF for the positioning module and 7 DOF for the surgery module, developed and fabricated for prostate brachytherapy [5]. In [6] another robotic system, entitled MIRAB is a 6-DOF robot capable of inserting and rotating 16 needles concurrently with a very high precision. G.S. Fischer et al introduced a 4-DOF hybrid robot for real-time control transperineal prostate needle orientation under MRI guidance and perform insertion motion manually [7]. Another study [8], presents a model-based dynamics equation for the needle movement through the soft tissue. The force estimation calculated through the simulated tissue deformation and the dynamic finite element as tissue model, is used as force feedback.

All the above mentioned aspects encourage a detailed study of the dynamic behavior of the proposed robotic structure to enable the definition of proper algorithms in the control system of the robot. Pierrot and Reynaud [9] propose a simplified method for the determination of the dynamic model of two parallel robotic structures, the DELTA and the HEXA robots. In [10] the authors applied the Lagrangian formalism for a 6-DOF fully parallel manipulator. The idea was to consider open-loop sub chains of the manipulator and to derive their dynamics by the Lagrangian formalism. In [11] are presented the kinematic and dynamic analyses, of a class of series–parallel manipulators, known as 2(3-RPS) manipulators. These analyses are approached via screw theory and the principle of virtual work. Khalil presents in [12] the inverse and direct dynamic models of different robotics systems based on the recursive Newton-Euler formulation. Staicu uses recursive matrix relations to develop the inverse kinematic and dynamic model of an orienting gear train mechanism [13, 14]. The fundamental principle of virtual work has been used to establish a direct recursive determination of the real-time variation of torques for the actuators.

In [15] the authors present a semi-automated robotic system with 5-DOF developed for brachytherapy procedures. The dynamic modelling of this structure is presented in this paper.

The paper is structured as follows: section 2 describes the mechanical structure of the robotic system; section 3 deals with the inverse dynamics analysis of the 5-DOF modular parallel mechanism using the principle of virtual work. A comparison of the numerical results obtained by the analytical approach and a multibody simulation software (Siemens NX) is also presented in order to validate the results. The conclusions of this work are presented in section 5, followed by the acknowledgements and references.

2. THE INNOVATIVE 5-DOF PARALLEL ROBOTIC STRUCTURE OF BRACHYTHERAPY

The modular parallel solution [15], proposed for development as a medical robot for brachytherapy specific tasks, like the procedure of the needle insertion in patient's bodies, consists of two different modules (Fig. 1). The first one has 3-DOF, based on a closed-loop structure, having a spatial construction and is used for positioning the mobile platform in the 3D space. The second module with 2-DOF is attached to the mobile platform and is used for the orientation of the end-effector.

The first module, of type 2CRR, is positioned on two lateral perpendicular sides of the fixed frame, on one side having two active joints: the translational joint q_1 and the rotational joint q_2. On the other side of the fixed frame (perpendicular to the first one) the module consists of an active translational joint q_3 and a passive rotational joint. Also the module has 4 revolute passive joints which connect the links in the kinematic chains and the mobile platform of the module. The orientation mechanism is connected to this

platform, consisting of two active joints, the rotational joint (q_4) and the active translational joint (q_5). The translational motion is transformed in rotational motion by a parallel mechanism (Fig. 1), consisting of two passive rotational joints and three links (e_3, d_5 and $d_6 + d_7$). Through the motion of the two parallel modules, the BT needle can be positioned and oriented based on the application requirements.

Having a separate orientation module fixed to the mobile platform of the positioning module, this robot does not need a guiding system in order to work properly, the positioning and orientation of the end-effector being achieved by means of five motors. Therefore the 5-DOF modular parallel robot has the advantage it can guide and introduce the needles into the patient body. The kinematic representation of the robotic structure with 5-DOF is shown in Fig. 1. The robot's main task is the positioning and orientation of its end effector, which holds the BT needles and introduces them into the patient's body, based on the oncologist's control commands. In kinematics terms, this refers to the positioning of a target point $E(X_E, Y_E, Z_E)$ in a 3D space, following an imposed path.

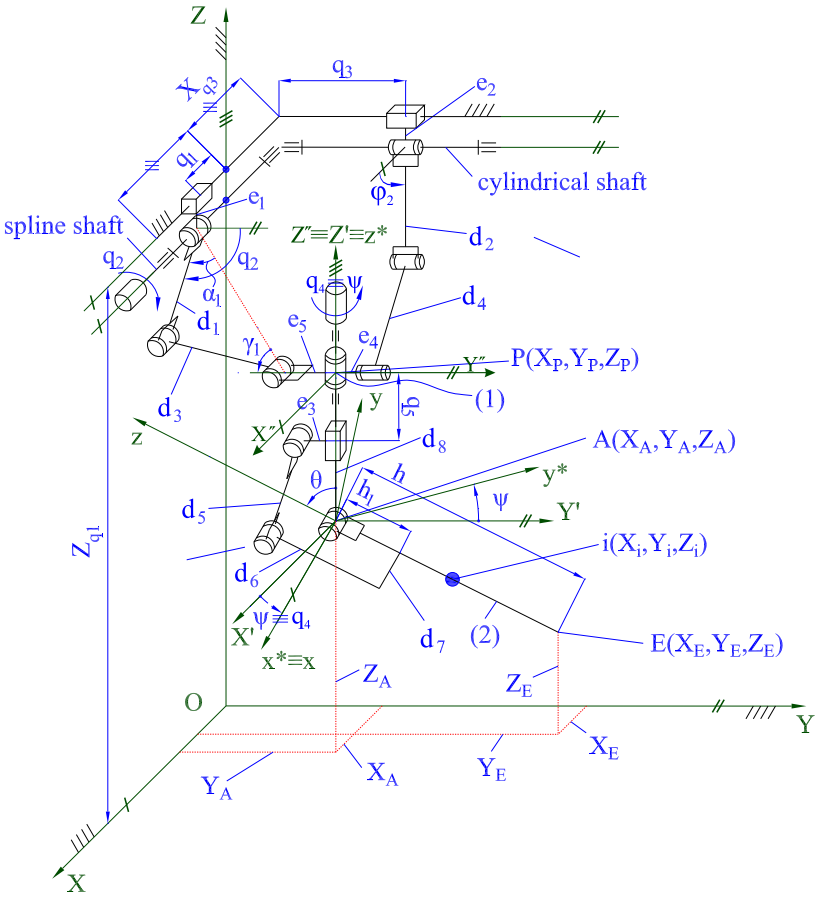

Fig. 1 – The kinematic scheme of the robot.

The implicit functions which characterize the relation between the coordinates of the end-effector, X_{PE} and the active joints, q:

$$F_1(q_1, X_E, \psi, \theta) \equiv q_1 - X_E + h \cdot \sin(\theta) \cdot \sin(\psi) = 0$$

$$F_2(q_2, Y_E, Z_E, \psi, \theta) \equiv q_2 - \operatorname{asin}\left(\frac{Z_{q_1} - e_1 - T_8 - Z_E - h \cdot \cos(\theta)}{\sqrt{\left(Y_{q_2} + e_5 - Y_E + h \cdot \sin(\theta) \cdot \cos(\psi)\right)^2 + \left(Z_{q_1} - e_1 - T_8 - Z_E - h \cdot \cos(\theta)^2\right)}} \right) \quad (1)$$

$$F_3(q_3, Y_E, \psi, \theta) \equiv q_3 - e_4 - Y_E + h \cdot \sin(\theta) \cdot \cos(\psi) = 0$$

$$F_4(q_4, \psi) \equiv q_4 - \psi = 0 \,.$$

$$F_5(q_5, Z_E, \theta) \equiv q_5 - Z_E - h \cdot \cos(\theta) - \left(T_6 \cdot \cos(\theta) - \sqrt{h_1^2 + T_7^2} \cdot \cos\left(\theta - \operatorname{atan}\left(\frac{T_7}{h_1} \right) \right) \right) -$$

$$- \sqrt{T_5^2 - \left(T_6 \cdot \sin(\theta) - \sqrt{h_1^2 + T_7^2} \cdot \sin\left(\theta - \operatorname{atan}\left(\frac{T_7}{h_1} \right) \right) - e_3 \right)^2} = 0$$

3. THE INVERSE DYNAMIC MODEL

The fundamental principle of the virtual work states that a mechanism is under dynamic equilibrium if and only if the total virtual work developed by all external, internal and inertia forces vanish during any general virtual displacement, which is compatible with the constraints imposed on the mechanism.

The inverse dynamic model, developed in this section, is critical for the studied kinematic structure (Fig. 1), considering that the 5 DOF robot is used in medical applications for needle insertion, especially in brachytherapy, meaning that the robot will be in direct contact with the human tissues.

The inputs for the generation of the inverse dynamic model are: the motion laws of the robot's end effector on the three coordinates, the inverse kinematic model, the masses of the robot elements and the outputs are the forces/torques at the level of the actuators.

Starting from the principle of lumped masses, the 28 elements of the robot were concentrated in 20 components, having the masses M_i, $i = 1...20$, which were divided in 28 lumped masses, with a distribution as is described in Figs. 2 and 3. The friction forces have been neglected and only the forces and moments introduced by the mechanical parts were considered. The following elements are considered:

- The components which build up the sliding parts of the linear actuators (q_1 and q_3, Fig. 1) having the masses M_1 and M_6, consists of the actuator's sliders (1) and (7) with masses M_{slider} and the connecting elements (2) and (8), with masses M_{con_el};
- The rods of the positioning module (3), (5), (10) and (12), having the masses M_2, M_4, M_8 and M_{10};
- The coupling elements of the rods (4), (6), (9) and (11), with the masses M_3, M_5, M_7 and M_9;
- The mobile platform of the positioning module (13), including the bearings (14) and the fixing elements (15) of the actuator q_4, having the mass M_{11};
- The actuator (the motor (16), the gearbox (17) and the connection elements (18)) corresponding to the active joint q_4, with mass M_{12};
- The motor (19) and the gearbox (20) of the linear actuator for the active joint q_5, with mass M_{13};
- The support element of the linear actuator (21), with mass M_{14};
- The fixed part of the linear actuator (22) having the mass M_{15}, including the bearings and the screw;
- The components (23) and (24), which build up the sliding part of the linear actuator q_5, with mass M_{16};
- The rod (25) with mass M_{17}, which connect the slider of the linear actuator q_5 (23+24) and the final element of the orientation module (26);
- The final element of the orientation module (26) having the mass M_{18};
- The telescopic needle holder (27), with mass M_{19};
- The needle (28) having the mass M_{20}.

For the elements having the masses: M_1, M_3, M_5, M_6, M_7, M_9, M_{11}, M_{12}, M_{13}, M_{16}, the whole mass was concentrated in the center of mass of the element. The rest of the elements, namely those having the masses: M_2, M_4, M_8, M_{10}, M_{14}, M_{15}, M_{17}, M_{18}, M_{19}, M_{20} were considered homogenous bars. The m_i are the lumped masses of the robot elements and joints, where $i = 1...28$. Also, the coordinates of the lumped masses $X_i, Y_i, Z_i, i = 1...28$ are determined.

$$m_1 = M_1;\ m_2 = \frac{1}{6}M_2;\quad m_3 = \frac{2}{3}M_2;\ m_4 = \frac{1}{6}M_2 + M_3 + \frac{1}{6}M_4;\quad m_5 = \frac{2}{3}M_4;\ m_6 = \frac{1}{6}M_4 + M_5;$$

$$m_7 = M_6;\ m_8 = M_7 + \frac{1}{6}M_8;\quad m_9 = \frac{2}{3}M_8;\ m_{10} = \frac{1}{6}M_8 + M_9 + \frac{1}{6}M_{10};\ m_{11} = \frac{2}{3}M_{10};\ m_{12} = \frac{1}{6}M_{10};$$

$$m_{13}=M_{11};\ m_{14}=M_{12};\ m_{15}=M_{13};\ m_{16}=\frac{1}{6}M_{14}+\frac{1}{6}M_{15};\ m_{17}=\frac{2}{3}M_{14}+\frac{2}{3}M_{15};\ m_{18}=\frac{1}{6}M_{14}+\frac{1}{6}M_{15};$$

$$m_{19}=M_{16};\ \ m_{20}=\frac{1}{6}M_{17};\ \ m_{21}=\frac{2}{3}M_{17};\ \ m_{22}=\frac{1}{6}M_{17}+\frac{1}{9}M_{18};\ \ m_{23}=\frac{4}{9}M_{18};\ m_{24}=\frac{1}{6}M_{18};\ \ m_{25}=\frac{2}{9}M_{18};$$

$$m_{26}=\frac{1}{18}M_{18}+\frac{1}{6}M_{19}+\frac{1}{6}M_{20};\ \ m_{27}=\frac{2}{3}M_{19}+\frac{2}{3}M_{20};\ \ \ m_{28}=\frac{1}{6}M_{19}+\frac{1}{6}M_{20}$$

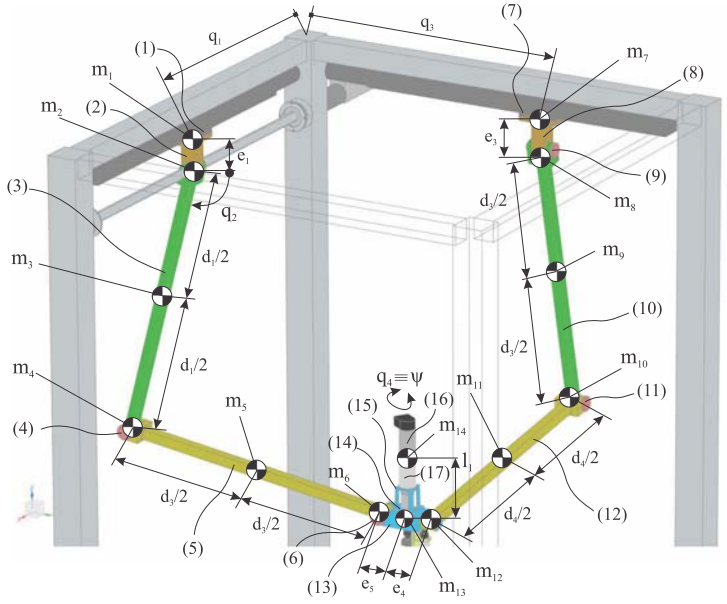

Fig. 2 – The distribution of the masses for the positioning module.

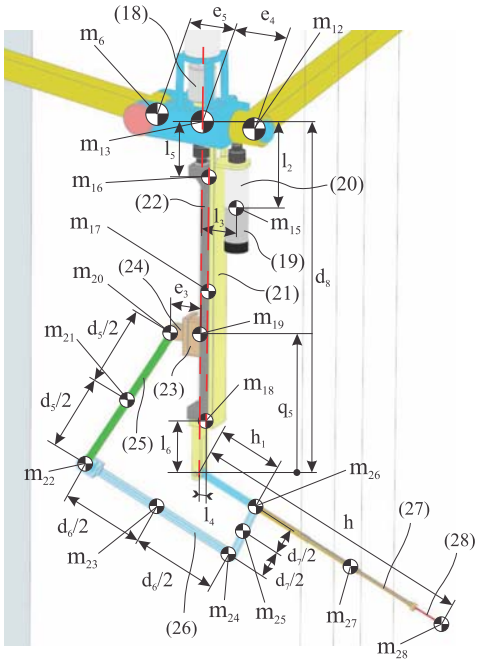

Fig. 3 – The distribution of the masses for the orientation module.

The coordinates of the concentrated mass points are:

$$X_1=q_1;\qquad Y_1=Y_{q1};\qquad Z_1=Z_{q1};\qquad \psi\equiv q_4$$

$$X_2=q_1;\qquad Y_2=Y_{q1};\qquad Z_2=Z_{q1}-e_1;$$

$$\begin{cases} X_3=q_1;\\ Y_3=Y_{q_1}+d_1/2\cdot\cos(q_2);\\ Z_3=Z_{q_1}-e_1-d_1/2\cdot\sin(q_2); \end{cases}\quad \begin{cases} X_4=q_1;\\ Y_4=Y_{q_1}+d_1\cdot\cos(q_2);\\ Z_4=Z_{q_1}-e_1-d_1\cdot\sin(q_2); \end{cases}\quad \begin{cases} X_9=X_{q3}+d_2/2\cdot\cos(\varphi_2);\\ Y_9=q_3;\\ Z_9=Z_{q3}-e_2-d_2/2\cdot\sin(\varphi_2); \end{cases}$$

$$\begin{cases} X_5=q_1;\\ Y_5=Y_{q_1}+d_1\cdot\cos(q_2)+\left(q_3-e_4-e_5-\left(Y_{q_1}+d_1\cdot\cos(q_2)\right)\right)/2\\ Z_5=Z_{q_1}-e_1-d_1\cdot\sin(q_2)-\sqrt{d_3^2-\left(q_3-e_4-e_5-\left(Y_{q_1}+d_1\cdot\cos(q_2)\right)\right)^2}\ \Big/2; \end{cases} \tag{3}$$

$$\begin{cases} X_6=q_1;\\ Y_6=q_3-e_4-e_5;\\ Z_6=Z_P; \end{cases}\quad \begin{cases} X_{10}=X_{q3}+d_2\cdot\cos(\varphi_2);\\ Y_{10}=q_3;\\ Z_{10}=Z_{q3}-e_2-d_2\cdot\sin(\varphi_2); \end{cases}\quad \begin{cases} X_7=X_{q3}\\ Y_7=Y_{q3}\\ Z_7=Z_{q3} \end{cases};\quad \begin{cases} X_8=X_{q3}\\ Y_8=Y_{q3}\\ Z_8=Z_{q3}-e_2 \end{cases};$$

$$\begin{cases} X_{11}=X_{q3}+d_2\cdot\cos(\varphi_2)+\left(q_1-\left(X_{q3}+d_2\cdot\cos(\varphi_2)\right)\right)/2;\\ Y_{11}=q_3;\\ Z_{11}=Z_{q3}-e_2-d_2\cdot\sin(\varphi_2)-\sqrt{d_4^2-\left(q_1-\left(X_{q3}+d_2\cdot\cos(\varphi_2)\right)\right)^2}\ /2; \end{cases}$$

where:

$$\varphi_2 = \operatorname{asin}\left(\frac{Z_{q3} - e_2 - Z_P}{L_{24}}\right) + \operatorname{acos}\left(\frac{d_2^2 + L_{24}^2 - d_4^2}{2 \cdot d_2 \cdot L_{24}}\right) \qquad \theta_2 = \left(\theta - \frac{\pi}{2}\right)$$

$$Z_P = Z_{q1} - e_1 - d_1 \cdot \sin(q_2) - \sqrt{d_3^2 - \left(q_3 - e_4 - e_5 - \left(Y_{q1} + d_1 \cdot \cos(q_2)\right)\right)^2}$$

$$L_{24} = \sqrt{\left(X_{q3} - q_1\right)^2 + \left(Z_{q3} - e_2 - \left(Z_{q1} - e_1 - d_1 \sin(q_2) - \sqrt{d_3^2 - \left(q_3 - e_4 - e_5 - \left(Y_{q1} + d_1 \cos(q_2)\right)\right)^2}\right)\right)^2}$$

$$\begin{cases} X_{12} = q_1; \\ Y_{12} = q_3; \\ Z_{12} = Z_P; \end{cases} \quad \begin{cases} X_{13} = q_1; \\ Y_{13} = q_3 - e_4; \\ Z_{13} = Z_P; \end{cases} \quad \begin{cases} X_{14} = q_1; \\ Y_{14} = q_3 - e_4; \\ Z_{14} = Z_P + l_1; \end{cases} \quad \begin{cases} X_{15} = q_1 - l_3 \cdot \sin(q_4); \\ Y_{15} = q_3 - e_4 + l_3 \cdot \cos(q_4); \\ Z_{15} = Z_P - l_2; \end{cases} \quad \begin{cases} X_{16} = q_1 - l_4 \cdot \sin(q_4); \\ Y_{16} = q_3 - e_4 + l_4 \cdot \cos(q_4); \\ Z_{16} = Z_P - l_5; \end{cases}$$

$$\begin{cases} X_{17} = q_1 - l_4 \cdot \sin(q_4); \\ Y_{17} = q_3 - e_4 + l_4 \cdot \cos(q_4); \\ Z_{17} = Z_P - l_5 - \dfrac{d_8 - l_5 - l_6}{2}; \end{cases} \quad \begin{cases} X_{18} = q_1 - l_4 \cdot \sin(q_4); \\ Y_{18} = q_3 - e_4 + l_4 \cdot \cos(q_4); \\ Z_{18} = Z_P - (d_8 - l_6); \end{cases} \quad \begin{cases} X_{19} = q_1; \\ Y_{19} = q_3 - e_4; \\ Z_{19} = Z_P - d_8 + q_5; \end{cases} \quad \begin{cases} X_{20} = q_1 + e_3 \cdot \sin(q_4); \\ Y_{20} = q_3 - e_4 - e_3 \cdot \cos(q_4); \\ Z_{20} = Z_P - d_8 + q_5; \end{cases}$$

$$\begin{cases} X_{21} = q_1 + (d_6 - h_1) \cdot \sin(\theta) \cdot \sin(q_4) - d_7 \cdot \sin(\theta_2) \cdot \sin(q_4) - (d_5/2) \cdot \sin(\theta + \alpha_7 + \alpha_8) \cdot \sin(q_4); \\ Y_{21} = q_3 - e_4 - (d_6 - h_1) \cdot \sin(\theta) \cdot \cos(q_4) + d_7 \cdot \sin(\theta_2) \cdot \cos(q_4) + (d_5/2) \cdot \sin(\theta + \alpha_7 + \alpha_8) \cdot \cos(q_4); \\ Z_{21} = Z_P - d_8 + (d_6 - h_1) \cdot \cos(\theta) - d_7 \cdot \cos(\theta_2) - (d_5/2) \cdot \cos(\theta + \alpha_7 + \alpha_8); \end{cases}$$

where:

$$\alpha_7 = \frac{\pi}{2} - \operatorname{acos}\left(\frac{\mathrm{d}_7}{\sqrt{\mathrm{d}_7^2 + (d_6 - h_1)^2}}\right) \qquad \alpha_8 = \operatorname{acos}\left(\frac{\mathrm{d}_7^2 + (d_6 - h_1)^2 + \mathrm{d}_5^2 - \mathrm{e}_3^2 - q_5^2}{2 \cdot d_5 \cdot \sqrt{\mathrm{d}_7^2 + (d_6 - h_1)^2}}\right)$$

$$\theta = \operatorname{atan}\left(\frac{\mathrm{e}_3}{\mathrm{q}_5}\right) + \operatorname{acos}\left(\frac{\mathrm{e}_3^2 + q_5^2 + d_7^2 + (d_6 - h_1)^2 - d_5^2}{2 \cdot \sqrt{\mathrm{e}_3^2 + q_5^2} \cdot \sqrt{\mathrm{d}_7^2 + (d_6 - h_1)^2}}\right) + \operatorname{acos}\left(\frac{\mathrm{d}_7}{\sqrt{\mathrm{d}_7^2 + (d_6 - h_1)^2}}\right) - \frac{\pi}{2}$$

$$\begin{cases} X_{22} = q_1 + (d_6 - h_1) \cdot \sin(\theta) \cdot \sin(q_4) - d_7 \cdot \sin(\theta_2) \cdot \sin(q_4); \\ Y_{22} = q_3 - e_4 - (d_6 - h_1) \cdot \sin(\theta) \cdot \cos(q_4) + d_7 \cdot \sin(\theta_2) \cdot \cos(q_4); \\ Z_{22} = Z_P - d_8 + (d_6 - h_1) \cdot \cos(\theta) - d_7 \cdot \cos(\theta_2); \end{cases} \quad \begin{cases} X_{26} = q_1 - h_1 \cdot \sin(\theta) \cdot \sin(q_4); \\ Y_{26} = q_3 - e_4 + h_1 \cdot \sin(\theta) \cdot \cos(q_4); \\ Z_{26} = Z_P - d_8 - h_1 \cdot \cos(\theta); \end{cases}$$

$$\begin{cases} X_{23} = q_1 + (d_6/2 - h_1) \cdot \sin(\theta) \cdot \sin(q_4) - d_7 \cdot \sin(\theta_2) \cdot \sin(q_4); \\ Y_{23} = q_3 - e_4 - (d_6/2 - h_1) \cdot \sin(\theta) \cdot \cos(q_4) + d_7 \cdot \sin(\theta_2) \cdot \cos(q_4); \\ Z_{23} = Z_P - d_8 + (d_6/2 - h_1) \cdot \cos(\theta) - d_7 \cdot \cos(\theta_2); \end{cases}$$

$$\begin{cases} X_{24} = q_1 - h_1 \cdot \sin(\theta) \cdot \sin(q_4) - d_7 \cdot \sin(\theta_2) \cdot \sin(q_4); \\ Y_{24} = q_3 - e_4 + h_1 \cdot \sin(\theta) \cdot \cos(q_4) + d_7 \cdot \sin(\theta_2) \cdot \cos(q_4); \\ Z_{24} = Z_P - d_8 - h_1 \cdot \cos(\theta) - d_7 \cdot \cos(\theta_2); \end{cases} \quad \begin{cases} X_{27} = q_1 - (h_1 + h) \cdot \sin(\theta) \cdot \sin(q_4)/2; \\ Y_{27} = q_3 - e_4 + (h_1 + h) \cdot \sin(\theta) \cdot \cos(q_4)/2; \\ Z_{27} = Z_P - d_8 - (h_1 + h) \cdot \cos(\theta)/2; \end{cases}$$

$$\begin{cases} X_{25} = q_1 - h_1 \cdot \sin(\theta) \cdot \sin(q_4) - (d_7/2) \cdot \sin(\theta_2) \cdot \sin(q_4); \\ Y_{25} = q_3 - e_4 + h_1 \cdot \sin(\theta) \cdot \cos(q_4) + (d_7/2) \cdot \sin(\theta_2) \cdot \cos(q_4); \\ Z_{25} = Z_P - d_8 - h_1 \cdot \cos(\theta) - (d_7/2) \cdot \cos(\theta_2); \end{cases} \quad \begin{cases} X_{28} = q_1 - h \cdot \sin(\theta) \cdot \sin(q_4); \\ Y_{28} = q_3 - e_4 + h \cdot \sin(\theta) \cdot \cos(q_4); \\ Z_{28} = Z_P - d_8 - h \cdot \cos(\theta). \end{cases}$$

Using the principle of the virtual displacements, the virtual work is defined:

$$\delta W = \delta q^T \cdot \tau + \sum_{i=1}^{28} \delta X_{mi}^T \cdot \left(T_i^{Tr} + T_i^g\right) = 0, \tag{4}$$

where $\delta q^T \cdot \tau$ is the virtual work of all the actuating forces and moments and $\sum_{i=1}^{28} \delta X_{mi}^T \cdot \left(T_i^{Tr} + T_i^g\right)$ is the sum of the virtual work obtained from the inertial forces and gravitational forces corresponding to the equivalent system (with 28 lumped masses). The matrices of the inertial forces and gravity are:

$$T_i^{Tr} = \begin{bmatrix} -m_i \cdot \ddot{X}_i \\ -m_i \cdot \ddot{Y}_i \\ -m_i \cdot \ddot{Z}_i \end{bmatrix} \equiv -\begin{bmatrix} m_i & 0 & 0 \\ 0 & m_i & 0 \\ 0 & 0 & m_i \end{bmatrix} \begin{bmatrix} \ddot{X}_i \\ \ddot{Y}_i \\ \ddot{Z}_i \end{bmatrix} \equiv -M_i \cdot \ddot{X}_{m_i}, T_i^g = \begin{bmatrix} 0 \\ 0 \\ -m_i \cdot g \end{bmatrix} \equiv -M_i \cdot v_g, i = 1...28, v_g = \begin{bmatrix} 0 \\ 0 \\ g \end{bmatrix}. \quad (5)$$

The sum of the inertial (4) and the gravitational (5) forces, which act in the robotic system is:

$$T_i = T_i^{Tr} + T_i^g \text{ or } T_i = -M_i \cdot \left(\ddot{X}_{m_i} + v_g \right). \quad (6)$$

The velocity vector of the 28 lumped masses and the velocity vector of the active joints q_i can be written:

$$\dot{X}_{PE} = J_E \cdot \dot{q} \text{ respectively } \dot{X}_{m_i} = J_i \cdot \dot{q}. \quad (7)$$

The time derivatives of the eq. (8) enable the determination of the acceleration vector, as follows:

$$\ddot{X}_{PE} = J_E \cdot \ddot{q} + \dot{J}_E \cdot \dot{q} \text{ respectively } \ddot{X}_{m_i} = J_i \cdot \ddot{q} + \dot{J}_i \cdot \dot{q}. \quad (8)$$

The virtual displacement at the level of the 28 points of lumped masses are defined with respect to the virtual displacements at the level of the active joints, using the eq. (8):

$$\delta X_{m_i} = J_i \cdot \delta q \text{ , and its transposed form } \delta X_{m_i}^T = \delta q^T \cdot J_i^T. \quad (9)$$

Substituting (6), (8) and (9) in the equation of the virtual work, eq. (4) becomes:

$$\delta W = \delta q^T \cdot \tau - \sum_{i=1}^{28} \delta q^T \cdot J_i^T \cdot M_i \cdot \left(\ddot{X}_{m_i} + v_g \right) = 0. \quad (10)$$

Simplifying (11) the equation that defines the torque vector of the actuators is:

$$\tau = \sum_{i=1}^{28} J_i^T \cdot M_i \cdot \left(\ddot{X}_{m_i} + v_g \right). \quad (11)$$

4. SIMULATION RESULTS AND VALIDATION OF INVERSE DYNAMICS WITH SIEMENS NX

In order to position the needle in the interest area, the physician's gives a set of coordinates for the insertion and the target points, which defines a simple motion for the end-effector, a linear displacement between these defined points. The simulations studied the robot capabilities of moving the end-effector, following a linear trajectory between two points in space.

The simulated trajectory (Fig. 4) represents **a linear displacement** of the end-effector **between two points in space**. The trajectory was defined by the following coordinates in space, which represents the insertion point $X_i = -23.0$ mm, $Y_i = 462.0$ mm, $Z_i = 960.0$ mm and the target point $X_t = -53.0$ mm, $Y_t = 544.0$ mm, $Z_t = 912.0$ mm. This simulated trajectory is similar to a real medical procedure.

By comparing the simulation plots for the inverse dynamic model (IDM – MATLAB and MBS – Siemens NX), the results have shown a very good correlation between the curves, where the forces/torques corresponding to the motors q_1, q_2, q_3, q_4 and q_5 have the same rate (shape).

This validates the inverse dynamics model developed in this paper and shown that this simplified analytical model can be implemented in the control algorithm of the robot.

5. CONCLUSIONS

The paper presents the inverse dynamic modeling of a modular parallel robot with 5 DOF, which could be used for medical applications, namely for brachytherapy. Starting from the mass geometry consideration,

which consists in replacing correctly the given multi-body system with dynamically equivalent lumped masses, the principle of virtual work was proposed in order to develop the inverse dynamics. The advantage of this approach consists in obtaining the inverse dynamic model in an analytical way. The achieved dynamic model, using the principle of virtual work is based on a fast computing algorithm, which enable its implementation in the control system of the robot.

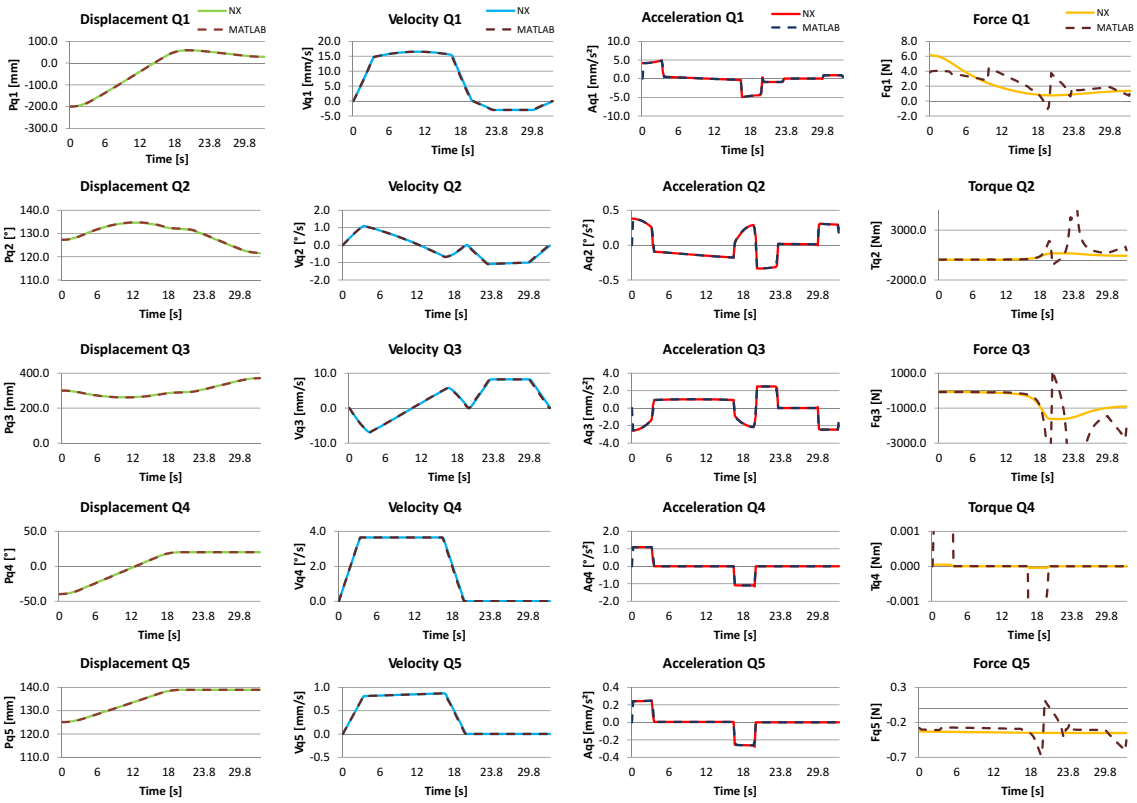

Fig. 4 – Simulation results for a linear displacement between two points in space.

ACKNOWLEDGEMENTS

This paper was supported by the project no. 173/2012, code PN-II-PCCA-2011-3.2-0414, entitled „Robotic assisted brachytherapy, an innovative approach of inoperable cancers – CHANCE" and the Bilateral Austria – Romania Project 745/2014, entitled "Developing methods to evaluate the accuracy of potential parallel robots for medical applications" both financed by UEFISCDI.

REFERENCES

1. STRASSMAN, G., *et al*., *Advantage of robotic needle placement on a prostate model in HDR brachytherapy*, Strahlenther Onkol., **187**, 6, pp. 367–272, 2011.
2. PODDER, T.K., FICHTINGER, G., *Robotic Brachytherapy – Overview*, AAPM Annual Meeting, July 19, 2010.
3. NEDEZKI, C.M., *The maximal workspace with constant orientation of the 3 dof RPR parallel manipulator*, Acta Tehnica Napocensis, **56** (IV), pp.725–728, 2013.
4. BASSAN, H., HAYES, T., PATEL, R.V., MOALLEM, M., *A Novel Manipulator for 3D Ultrasound Guided Percutaneous Needle Insertion*, IEEE International Conference on Robotics and Automation, pp. 617–622, 2007.
5. YU, Y. *et al*., *Robot-Assisted Prostate Brachytherapy*, MICCAI, **9**, *1*, pp. 41–49, 2006.
6. PODDER, T., et al, *MIRAB: An Image-Guided Multichannel Robot for Prostate Brachytherapy*, Bodine Journal, **3**, *1*, 2010.
7. FISCHER, G.S., et al, *Design of a Robot for Transperineal Prostate Needle Placement in MRI Scanner*, IEEE International Conference on Mechatronics, pp. 592–597, DOI 10.1109/ICMECH.2006.252593, 2006.
8. MAGHSOUDI, A., JAHED, M.: *Needle dynamics modelling and control in prostate brachytherapy*, IET Control Theory & Applications, **6**, *11*, pp. 1671–1681, DOI: 10.1049/iet-cta.2011.0449, 2012.

9. PIERROT, F., *et al*., *A New Design of a 6-DOF Parallel Robot*, Journal of Robotics and Mechatronics, **2**, pp. 92–99, 1990.
10. ABDELLATIF, H., HEIMANN, B., *Computational efficient inverse dynamics of 6-DOF fully parallel manipulators by using the Lagrangian formalism*, Mechanism and Machine Theory, **44**, *1*, pp. 192–207, 2009.
11. GALLARDO-ALVARADO, J., *et al.*, *Kinematics and dynamics of 2(3-RPS) manipulators by means of screw theory and the principle of virtual work*, Mechanism and Machine Theory, **43**, *10*, pp. 1281–1294, 2008.
12. KHALIL, W., *Dynamic Modeling of Robots Using Newton-Euler Formulation*, Informatics in Control, Automation and Robotics, **89**, pp. 3–20, 2010.
13. STAICU, S., ZHANG, D.: *A novel dynamic modelling approach for parallel mechanisms analysis* Robotics and Computer-Integrated Manufacturing, **24**, *1*, pp. 167–172, 2008.
14. STAICU, S.: *Dynamics of a 2-DOF orienting gear mechanism,* Revue Roumaine des Sciences Techniques, **54**, *1*, pp. 67–77, 2009.
15. PLITEA, N., SZILAGHYI, A., PISLA, D.: *Kinematic Analysis of a new 5-DOF Modular Parallel Robot for Brachytherapy*, Robotics and Computer Integrated Manufacturing, **31**, pp. 70–80, 2015.

Received December 8, 2014